Proceedings of the
Annual Stability Conference
Structural Stability Research Council
San Antonio, Texas, March 19-22, 2024

Constrained Finite Strip Method: kinematic- and force-based approaches

Sheng Jin[1], Sándor Ádány[2,3], Benjamin W. Schafer[4]

Abstract
In recent decades constrained finite strip/element methods were introduced to perform modal identification and/or decomposition analysis of thin-walled members. Originally, the constraint equations were based – primarily – on kinematic equations to establish the deformation classes, such as global, distortional, local, etc. Lately, a new concept was introduced, where the modal classes are derived from specially defined forces acting on the member. In this novel approach the basis system of a mode class is obtained by solving the member's equilibrium equation under specialized forces, which requires the flexibility matrix. These two approaches, i.e., the kinematic-based and the force-based decomposition approaches are built on distinctly different mechanical ideas, still, they both provide similar capabilities for examining and understanding thin-walled members. In this paper, the new force-based method is introduced and applied in the context of the semi-analytical finite strip method. Numerical examples are provided to illustrate the similarities and important differences between the force-based and kinematic-based decomposition approaches.

1. Introduction

The application of modal decomposition in the buckling analysis of thin-walled members has proven to be an efficient tool both in improving understanding of behavior, and in improving computational efficiency. Modal decomposition separates the general displacement field into specific mode classes. Usually, three major modal classes are introduced: global (G), distortional (D) and local (L), but depending on the specific modal decomposition method, further sub-spaces might be necessary and/or useful to define (e.g. other (O) modes associated with shear and transverse extension). In the pioneering modal decomposition methods, such as the constrained Finite Strip Method (cFSM) and constrained Finite Element Method (cFEM), the modes are defined (essentially) by geometric constraints, see e.g. Ádány and Schafer (2008), and are similar to the definitions employed in Generalized Beam Theory, see e.g., Ádány et al. (2009). Although the kinematic-based modal decomposition helps to understand the deformations of a thin-walled member, and the method can be a useful tool in practical design, it has some disadvantages and

[1] Assoc. Professor, Chongqing University, <civiljs@cqu.edu.cn>
[2] Assoc. Research Scientist, Johns Hopkins University, <asandor2@jhu.edu>
[3] Professor, Budapest University of Technology and Economics, <adany.sandor@emk.bme.hu>
[4] Professor, Johns Hopkins University, <schafer@jhu.edu>

limitations. In the case of curved cross-sections, for example, the kinematic-based constraints do not work in a meaningful way, that is why special considerations are needed if cFSM is applied for cold-formed steel members with rounded corners (Beregszászi and Ádány, 2019), or, that is why specific modes are necessary to introduce in GBT if the cross-section is curved, see e.g., Nedelcu (2023).

Besides employing kinematic criteria to obtain the deformation classes, other approaches are possible. In Khezri and Rasmussen (2019a,b) the modal decomposition is based on energy considerations. Force-based modal decomposition was proposed by Jin (Jin et al, 2021a,b) and also by Becque (Becque and Davison, 2021). In this paper a newer variant of the force-based approach is applied and discussed in comparison with the original cFSM approach. To be able to easily distinguish between the two approaches, new acronyms are introduced: the original, *kinematic*-based approach will be referred to as *k*cFSM, while the *force*-based approach will be referred to as *f*cFSM. The acronym also is intended to partially imply the direct use of the stiffness matrix in the *k*cFSM and the flexibility matrix (i.e., the inverse of the stiffness matrix), in the *f*cFSM.

This paper begins, in Section 2, with the basics of both approaches. Then, in Section 3, the *f*cFSM is presented in a more detailed way, and applied to solve a classic buckling problem of a channel section column. As it will turn out, in the case of such simple problems *f*cFSM and *k*cFSM are found to lead to rather similar results. However, in Section 4 further examples are presented and discussed, which highlight the important differences between the two approaches.

2. *k*cFSM and *f*cFSM basics

The goal in the semi-analytical finite strip method (FSM) is to perform linear buckling analysis (LBA) for prismatic thin-walled structural members. The following generalized eigen-value problem is to be solved:

$$\boldsymbol{K_e \delta} = \lambda \boldsymbol{K_g \delta} \tag{1}$$

where $\boldsymbol{K_e}$ and $\boldsymbol{K_g}$ is the elastic and geometric stiffness matrix, respectively, $\boldsymbol{\delta}$ is an eigenvector, and λ is the corresponding eigenvalue. The eigenvector, physically, is a displacement vector which gives the buckling shape, while the eigenvalue is a load multiplier (and the assumed stresses associated with the reference load are embedded in $\boldsymbol{K_g}$) which gives the load level where bifurcation of equilibrium occurs, called the critical load.

Regardless of the criteria employed (i.e., whether they are kinematic-based or force-based), the basis vectors of the sub-spaces must be defined. If the basis vectors of a given mode class are collected into the $\boldsymbol{C}^*$ constraint matrix, a linear transformation of the degrees of freedom (DOF)s can readily be completed, as:

$$\boldsymbol{\delta}^* = \boldsymbol{C}^* \boldsymbol{\varphi}^* \tag{2}$$

where $\boldsymbol{C}^*$ is the constraint matrix of a class, where the superscript "*" denotes the mode class, which can be "^{L}" (local), "^{D}" (distortional), "^{G}" (global), or other if any; $\boldsymbol{\delta}^*$ is a displacement vector (expressed by the usual FSM nodal displacements); and $\boldsymbol{\varphi}^*$ can be understood as the modal displacement vector for the class, expressed by modal degrees of freedom. Note, the number of

elements of $\boldsymbol{\delta}^*$ is equal to the number of nodal degrees of freedom of the problem, regardless of the mode class, while $\boldsymbol{\varphi}^*$ has fewer elements and the element number is dependent on the mode class.

Applying Eq. (2) for the linear buckling problem formulated by Eq. (1), the modal buckling problem can be written as:

$$([\boldsymbol{C}^*]^{\mathrm{T}}\boldsymbol{K}_{\boldsymbol{e}}\boldsymbol{C}^*)\boldsymbol{\varphi}^* = \lambda\left([\boldsymbol{C}^*]^{\mathrm{T}}\boldsymbol{K}_{\boldsymbol{g}}\boldsymbol{C}^*\right)\boldsymbol{\varphi}^* \quad \rightarrow \quad \boldsymbol{K}_{\boldsymbol{e}}^*\boldsymbol{\varphi}^* = \lambda\boldsymbol{K}_{\boldsymbol{g}}^*\boldsymbol{\varphi}^* \tag{3}$$

where $\boldsymbol{K}_{\boldsymbol{e}}^*$ and $\boldsymbol{K}_{\boldsymbol{g}}^*$ are reduced-size elastic and geometric stiffness matrices for the eigen-value problem constrained to space "*".

In *k*cFSM, the separation of global (G), distortional (D), local (L) and other (O) deformation modes are completed through enforcing one or more out of a set of largely kinematic criteria. The most important criteria are as follows.

- The in-plane shear strain is zero.
- The transverse normal strain is zero.
- The warping has linear distribution along the width of a flat plate element.
- The warping is nonzero.
- The cross-section is undistorted.

Further criteria and sub-classes within G, L, and O have been introduced, see Ádány and Schafer (2014); however, the above criteria are the most crucial.

On the other hand, *f*cFSM categorizes the mode classes based on orthogonality criteria and force-displacement relationships, as shown by the four criteria of *f*cFSM:

- Criterion #1: The GD mode class is defined by the displacements of the member calculated from mid-line direction transverse forces, uniformly distributed in each wall.
- Criterion #2: The displacements for the D mode class are within the GD class, and the loads are distributed so that they are self-balanced.
- Criterion #3: G, D and L classes span the whole deformation space of a member.
- Criterion #4: G, D and L classes are orthogonal to each other with respect to the stiffness or flexibility matrix of the member.

The different mode class criteria of *k*cFSM and *f*cFSM lead to different constraint matrices, hence, the modal analysis results may be different. The similarities and differences in the two approaches is illustrated in the following sections through examples.

3. Lipped channel column

3.1 Example summary

An axially compressed steel lipped channel column is considered. The section has a web height of 120 mm, a flange width of 80 mm, a lip length of 15 mm, and a thickness of 1 mm. A customized version of the CUFSM software (CUFSM, 2023) is used for the buckling analysis of the member. The finite strip model is depicted in Fig. 1.

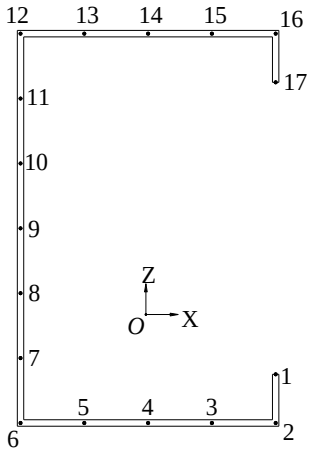

Figure 1: The finite strip model of a lipped channel C120×80×15×1: the nodes and the coordinate system

The material is assumed to be linear elastic, isotropic, with a Young's modulus of 210 GPa and Poisson's ratio of 0.3. In terms of the mesh, the web consists of 6 strips, the flange of 4 strips, and the lip a single strip. The number of strip nodal lines in the model is 17.

3.2 Constraint matrix for GD in fcFSM

According to the *f*cFSM criteria, equilibrium equations need to be solved. The equilibrium equation can be expressed as:

$$\boldsymbol{p} = \boldsymbol{K_e}\boldsymbol{\delta} \tag{4}$$

The displacement vector $\boldsymbol{\delta}$ has 68 DOF, 4 for each nodal line: the *U*, *V*, *W* translations along the X, Y, and Z axes, and the θ rotation around the Y-axis. The $\boldsymbol{p}$ load vector consists of the corresponding nodal forces and moments N_X, N_Y, N_Z and T. The $\boldsymbol{K_e}$ stiffness matrix is 68×68.

According to Criteria #1 and #2, the assumed load is uniform transverse load along the wall lines, as illustrated in Fig. 2. First, the distributed wall forces must be transformed into equivalent nodal forces, which can be expressed in matrix format as:

$$\boldsymbol{p} = \boldsymbol{J}\boldsymbol{q} \tag{5}$$

where $\boldsymbol{q}$ contains the distributed load intensities, while $\boldsymbol{J}$ represents the transformation from wall forces to nodal forces.

According to Criterion #1 of *f*cFSM, $\boldsymbol{q}$ is built up from wall forces parallel to the midline of the cross-section plates (i.e. in the local *x* direction of a strip), see Fig 2. The example has 5 walls, $\boldsymbol{q}$ can be expressed as $\boldsymbol{q} = \{q_1, q_2, q_3, q_4, q_5\}^{\mathrm{T}}$. Moreover, any $\boldsymbol{q}$ vector can be expressed by the linear combination of the q_i basis vectors, so, the linear space of the wall forces is 5-dimensional. Criterion #1 states that the GD mode class (i.e., the union of G and D) is derived from the wall forces, therefore, the basis (displacement) vectors of the GD mode class can be achieved by (i) transforming the basis vectors of the wall forces into nodal forces by Eq. (5), then (ii) solving the equilibrium equation Eq. (4). If the $\boldsymbol{Q}^{\mathrm{GD}}$ matrix contains of the 5 basis vectors of the wall forces in its columns, then, the transformation into nodal line forces is:

$$\boldsymbol{P}^{\mathrm{GD}} = \boldsymbol{J}^{\mathrm{GD}}\boldsymbol{Q}^{\mathrm{GD}} \tag{6}$$

where $\boldsymbol{P}^{\mathrm{GD}}$ is a matrix with 5 columns, each column being a vector of nodal forces in the GD mode class. Dimension of the transformation matrix $\boldsymbol{J}^{\mathrm{GD}}$ is 68×5, the row number is the same as the DOF of the model, and the column number is the same to walls. Apparently, the rows in $\boldsymbol{J}^{\mathrm{GD}}$ corresponding to the longitudinal nodal forces N_{Y} and nodal moments T are all zeros. In addition, the X- and Z- direction nodal forces N_{X} and N_{Z} are determined by the intensity of the q acting on the wall where the node locates, e.g. the N_{X} of Node #14 (located in the middle of upper flange, which is evenly divided into four elements by the nodes) is $N_{\mathrm{X},14} = q_4 \times A_{\mathrm{flange}}/4$, thus the corresponding row of $\boldsymbol{J}^{\mathrm{GD}}$ should be $\{0, 0, 0, A_{\mathrm{flange}}/4, 0\}$.

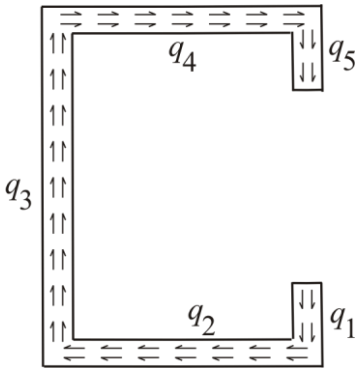

Figure 2: Distributed wall loads for GD mode class in *f*cFSM

From each of these column vectors the corresponding displacement vector can be calculated, formally expressed as:

$$\boldsymbol{\Delta}^{\mathrm{GD}} = \boldsymbol{K}_{\boldsymbol{e}}^{-1}\boldsymbol{P}^{\mathrm{GD}} = \boldsymbol{K}_{\boldsymbol{e}}^{-1}\boldsymbol{J}^{\mathrm{GD}}\boldsymbol{Q}^{\mathrm{GD}} \tag{7}$$

The obtained displacement vectors (in the columns of $\boldsymbol{\Delta}^{\mathrm{GD}}$) are the basis (displacement) vectors for the GD linear space, or, in other words, the column vectors of the $\boldsymbol{C}^{\mathrm{GD}}$ constraint matrix for the GD mode class. From Eq. (7) one can observe they are determined from the inverse of the stiffness matrix, also known as the flexibility matrix. Theoretically, the base system of the wall forces, i.e., the columns of the $\boldsymbol{Q}^{\mathrm{GD}}$ matrix, can be determined infinitely many ways; however, there is no reason not to use the trivial basis system which is composed of unit vectors. Therefore, $\boldsymbol{Q}^{\mathrm{GD}}$ can be equal to the 5×5 unit matrix, and the expression to calculate the GD constraint matrix simplifies to:

$$\boldsymbol{C}^{\mathrm{GD}} = \boldsymbol{K}_{\boldsymbol{e}}^{-1}\boldsymbol{J}^{\mathrm{GD}} \tag{8}$$

3.3 Constraint matrix for D in fcFSM

Per *f*cFSM criterion #2, D is a subset within the GD class where the loads on each cross-section are self-balanced. This means that any $\boldsymbol{q}$ in the D class, let us denote it as $\boldsymbol{q}^{\mathrm{D}}$, must satisfy the force (vertical and horizontal) and moment equilibrium equations, as follows:

$$\begin{cases} \left(q_1^{\mathrm{D}} + q_5^{\mathrm{D}}\right) \cdot A_{\mathrm{lip}} - q_3^{\mathrm{D}} \cdot A_{\mathrm{web}} & = 0 \\ q_2^{\mathrm{D}} - q_4^{\mathrm{D}} & = 0 \\ \left(q_1^{\mathrm{D}} + q_5^{\mathrm{D}}\right) \cdot A_{\mathrm{lip}} \cdot b + q_4^{\mathrm{D}} \cdot A_{\mathrm{flange}} \cdot h & = 0 \end{cases} \tag{9}$$

where A_{lip}, A_{web}, A_{flange} are, respectively, the cross-section area of a lip, a web, and a flange, and b and h are the width and height of the cross-section, respectively. In matrix format:

$$\boldsymbol{H}\boldsymbol{q}^{\mathrm{D}} = \boldsymbol{0} \tag{10}$$

where

$$\boldsymbol{H} = \begin{bmatrix} A_{\mathrm{lip}} & 0 & -A_{\mathrm{web}} & 0 & A_{\mathrm{lip}} \\ 0 & 1 & 0 & -1 & 0 \\ b \cdot A_{\mathrm{lip}} & 0 & 0 & h \cdot A_{\mathrm{flange}} & b \cdot A_{\mathrm{lip}} \end{bmatrix} \tag{11}$$

The above expression for $\boldsymbol{H}$ is valid for lipped channels only, however, it can easily be generalized to any cross-section. Once $\boldsymbol{H}$ is constructed, the basis vectors (of the wall forces) of the D mode class can be obtained as:

$$\boldsymbol{Q}^{\mathrm{D}} = \mathrm{nul}(\boldsymbol{H}) \tag{12}$$

Since D is part of GD, Eq. (7) can be applied to calculate the displacement basis vectors for D, i.e., the $\boldsymbol{C}^{\mathrm{D}}$ constraint matrix is obtained as:

$$\boldsymbol{C}^{\mathrm{D}} = \boldsymbol{K}_{\boldsymbol{e}}^{-1}\boldsymbol{J}^{\mathrm{GD}}\boldsymbol{Q}^{\mathrm{D}} = \boldsymbol{K}_{\boldsymbol{e}}^{-1}\boldsymbol{J}^{\mathrm{GD}}\mathrm{nul}(\boldsymbol{H}) \tag{13}$$

3.4 Constraint matrix for G in fcFSM

According to *f*cFSM Criterion #4, the vectors in the various spaces are orthogonal to each other with respect to the elastic stiffness matrix (i.e. deformations in one space do not create forces in another space). Considering the orthogonality between G and D, any $\boldsymbol{\delta}^{\mathrm{G}}$ displacement vector in the G mode class is orthogonal to any $\boldsymbol{\delta}^{\mathrm{D}}$ displacement vector in the D mode class as:

$$[\boldsymbol{\delta}^{\mathrm{D}}]^{\mathrm{T}}\boldsymbol{K}_{\boldsymbol{e}}\boldsymbol{\delta}^{\mathrm{G}} = 0 \quad \rightarrow \quad [\boldsymbol{\delta}^{\mathrm{D}}]^{\mathrm{T}}\boldsymbol{p}^{\mathrm{G}} = 0 \rightarrow [\boldsymbol{\delta}^{\mathrm{D}}]^{\mathrm{T}}\boldsymbol{J}^{\mathrm{GD}}\boldsymbol{q}^{\mathrm{G}} = 0 \tag{14}$$

To ensure Eq. (14) is satisfied for any $\boldsymbol{\delta}^{\mathrm{D}}$, apply the orthogonality equation to the basis displacement vectors of the D mode class:

$$[\boldsymbol{C}^{\mathrm{D}}]^{\mathrm{T}}\boldsymbol{J}^{\mathrm{GD}}\boldsymbol{q}^{\mathrm{G}} = \boldsymbol{0} \tag{15}$$

from which the basis vectors of the wall forces in the G mode class can be expressed as:

$$\boldsymbol{Q}^{\mathrm{G}} = \mathrm{null}([\boldsymbol{C}^{\mathrm{D}}]^{\mathrm{T}}\boldsymbol{J}^{\mathrm{GD}}) \tag{16}$$

Since G is part of GD, Eq. (7) can be applied to calculate the displacement basis vectors for G, i.e., the $\boldsymbol{C}^{\mathrm{G}}$ constraint matrix is obtained as:

$$\boldsymbol{C}^{\mathrm{G}} = \boldsymbol{K}_{\boldsymbol{e}}^{-1}\boldsymbol{J}^{\mathrm{GD}}\boldsymbol{Q}^{G} = \boldsymbol{K}_{\boldsymbol{e}}^{-1}\boldsymbol{J}^{\mathrm{GD}}\mathrm{null}([\boldsymbol{C}^{\mathrm{D}}]^{\mathrm{T}}\boldsymbol{J}^{\mathrm{GD}}) \tag{17}$$

3.5 Constraint matrix for L in fcFSM

According to Criterion #4, the vectors in the various spaces are orthogonal to each other through the elastic stiffness matrix. Considering the orthogonality between GD and L, any $\boldsymbol{\delta}^{\mathrm{L}}$ displacement vector in the L mode class is orthogonal to any $\boldsymbol{\delta}^{\mathrm{GD}}$ displacement vector in the GD mode class as:

$$[\boldsymbol{\delta}^{\mathrm{GD}}]^{\mathrm{T}}\boldsymbol{K}_{\boldsymbol{e}}\boldsymbol{\delta}^{\mathrm{L}} = 0 \tag{18}$$

To make sure that the above equation is satisfied to any $\boldsymbol{\delta}^{\mathrm{GD}}$, apply the orthogonality equation to the basis displacement vectors of the GD mode class:

$$[\boldsymbol{C}^{\mathrm{GD}}]^{\mathrm{T}}\boldsymbol{K}_{\boldsymbol{e}}\boldsymbol{\delta}^{\mathrm{L}} = \mathbf{0} \tag{19}$$

Considering Eq. (8), and utilizing that the stiffness matrix is symmetric:

$$[\boldsymbol{K}_{\boldsymbol{e}}^{-1}\boldsymbol{J}^{\mathrm{GD}}]^{\mathrm{T}}\boldsymbol{K}_{\boldsymbol{e}}\boldsymbol{\delta}^{\mathrm{L}} = \mathbf{0} \;\rightarrow\; [\boldsymbol{J}^{\mathrm{GD}}]^{\mathrm{T}}[\boldsymbol{K}_{\boldsymbol{e}}^{-1}]^{\mathrm{T}}\boldsymbol{K}_{\boldsymbol{e}}\boldsymbol{\delta}^{\mathrm{L}} = 0 \;\rightarrow\; [\boldsymbol{J}^{\mathrm{GD}}]^{\mathrm{T}}\boldsymbol{\delta}^{\mathrm{L}} = 0 \tag{20}$$

from which the displacement basis vectors for L, i.e., the $\boldsymbol{C}^{\mathrm{L}}$ constraint matrix is obtained as:

$$\boldsymbol{C}^{\mathrm{L}} = \mathrm{null}([\boldsymbol{J}^{\mathrm{GD}}]^{\mathrm{T}}) \tag{21}$$

Note, this definition of the L space would seem to be expansive, as all deformations that are not GD are defined as L. As the examples will illustrate, the reality is more subtle.

3.6 Unconstrained and constrained signature curves

For the given lipped channel column, the calculations of the signature curves were determined by a customized version of the CUFSM software, employing various options around *k*cFSM and *f*cFSM. The results are summarized in Fig. 3, where the first (lowest) critical load values are plotted as a function of the buckling half-wavelength, l_o.

- 'FSM signature' is the unconstrained solution, obtained from Eq. (1).
- 'L-*k*cFSM', 'D-*k*cFSM', and 'G-*k*cFSM' are constrained solutions, by solving Eq. (3) constrained into pure L, pure D, and pure G, respectively, and the constraint matrices are defined by the kinematic-based criteria.
- 'L-*f*cFSM', 'D-*f*cFSM', and 'G-*f*cFSM' are constrained solutions, by solving Eq. (3) constrained into pure L, pure D, and pure G, respectively, and the constraint matrices are defined by the force-based criteria, given by Eqs. (13), (17) and (21).

In addition, modal identification of the FSM signature solution is performed by the two methods and compared in Fig. 3. It can be found from Fig. 3 that although the criteria for modal definitions in *k*cFSM and *f*cFSM are different, their modal buckling analyses lead to nearly identical solutions.

Since this example is well-known, it does not require a detailed discussion. In general, the signature curves and modal participations are in accordance with earlier results, discussed in earlier papers.

As far as the modal decomposition is concerned, the general observation is that the results from *k*cFSM and *f*cFSM are very similar. No discrepancy can be observed between the L solutions of the two methods, and the pure L buckling solutions match well with the FSM signature curve in the l_0 < 300mm region. This is remarkable, since the L modes in the two approaches are so

differently defined. In *k*cFSM, the warping of L class is prescribed to be zero. As a result, mid-line direction translations of all the nodes are zero due to the null in-plane shear strain assumption. In *f*cFSM, the L class is deduced from the orthogonality to GD class where the intensity of the evenly distributed mid-line direction force on a wall can be an arbitrary value, which means the virtual work done by this force on the L mode deformation should be zero. As a result, in *f*cFSM the average mid-line direction translation of each wall of the L class should be zero. This is not exactly the same as in *k*cFSM, but this difference has no noticeable effects in this example.

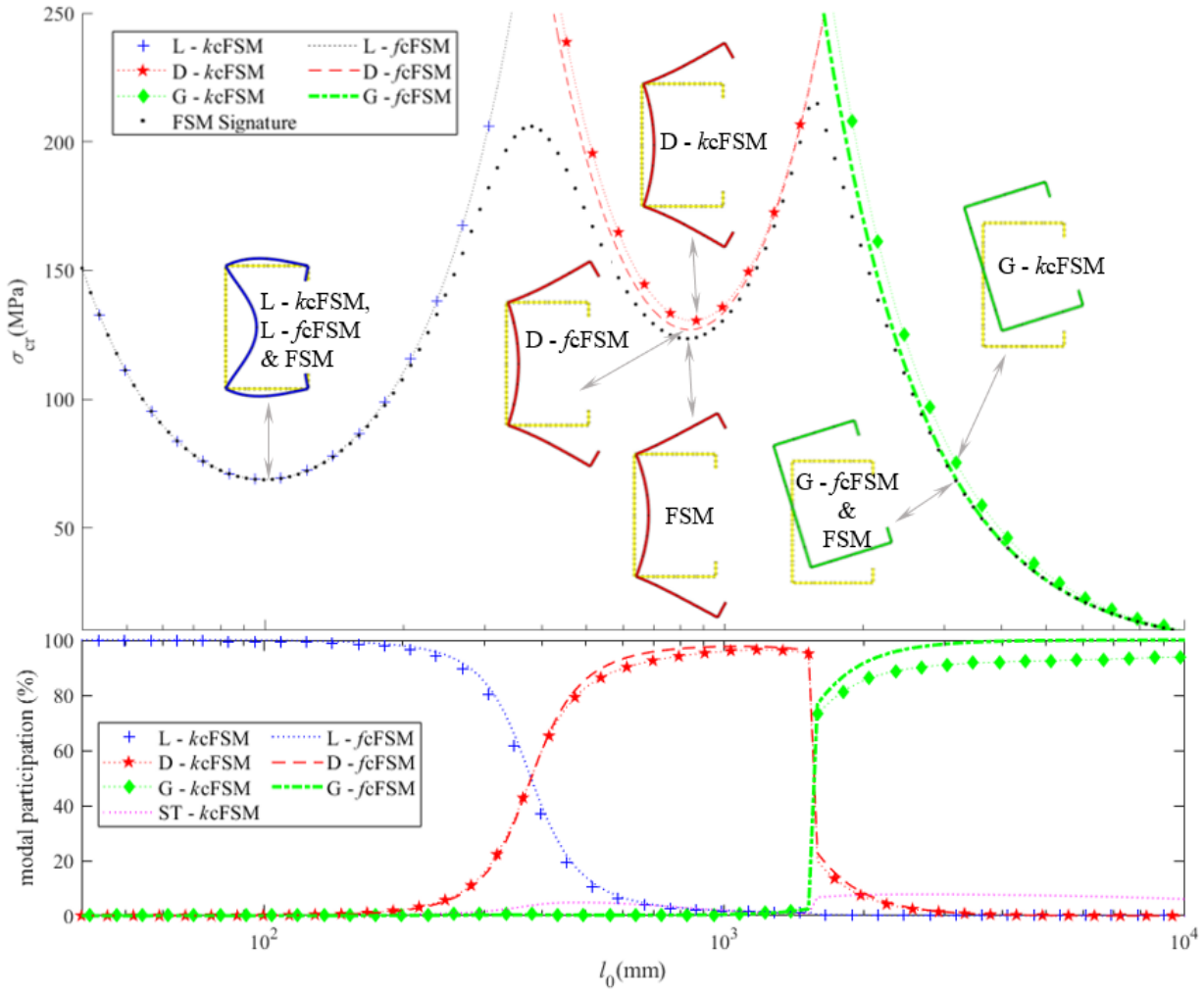

Figure 3: Signature curves and modal participations, section without extra supports

The D and G solutions are basically consistent between the *k*cFSM and *f*cFSM, both the signature curves and the buckled shapes. The *k*cFSM critical values are always higher, which is primarily due to the fact that in *k*cFSM the transverse extensions are forced to be zero, which results in a slightly increased axial rigidity of the plate elements of member. More generally, the transverse extensions and in-plane shear deformations are totally excluded from the GD class of *k*cFSM (and handled in separate classes), while in *f*cFSM small transverse extensions and in-plane shear are allowed, and in fact, exist within the G and D classes.

4. Lipped channel column with extra supports

4.1 Example summary

The example is a direct extension to that of Section 3. However, transverse springs are added to the web and bottom flange, as might exist due to bracing or attachment along the length of a member, as shown in Fig. 4. The spring stiffness values vary, and will be specified below.

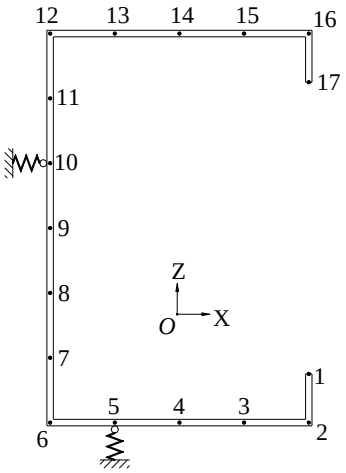

Figure 4: The member with extra springs

4.2 The effect of elastic springs in cFSM

In the case of *k*cFSM the definition of the modal basis vectors (i.e., the calculation of the constraint matrices) is dependent on the cross-section geometry only, hence, it is independent of the supports in general, or independent of added springs in this specific example. As far as the constraint buckling solutions are concerned, therefore, $\boldsymbol{C}^*$ is not affected by the added springs, $\boldsymbol{K_g}$ is unchanged, too (since in the implementation of the semi-analytical FSM the initial stress state is assumed, not calculated), however, $\boldsymbol{K_e}$ is modified: the spring stiffnesses are added to the corresponding elements of the elastic stiffness matrix. Accordingly, the constrained signature curves and the modal participations will be different.

In the case of *f*cFSM, the elastic stiffness or flexibility matrix has a prominent role in calculating the $\boldsymbol{C}^*$ constraint matrices, as can be observed from the derivations in Section 3. Consequently, not only the constrained signature curves and modal participations, but the G-D-L spaces will be different compared to the case without the extra spring supports.

4.3 Unconstrained and constrained signature curves with elastic springs

The signature curves and modal participations have been recalculated with the springs included. The spring stiffness is set to 5.0 N/mm/mm. The same options have been used as in Section 3. The obtained results are summarized in Fig. 5.

By adding the support springs the elastic buckling loads increase, and the unconstrained signature curve moves up. The general shape of the signature curve remains the same, though in the range of medium half-wavelengths the shape of the signature curve is slightly changed and the buckling shape is modified as well.

The unconstrained (FSM signature) and pure *f*cFSM D buckling modes are similar, and they are clearly different from the shape in the example without springs. In fact, the buckled shapes are similar to the D buckling of a beam problem (which is not surprising: the springs reduce the displacement of the lower flange zone, similarly to the tensile stresses in a beam). The pure *k*cFSM D buckling mode is similar to a point-symmetric D mode, which is typically the second D mode in unsupported members; however, the symmetric D mode is now excluded by the spring supports.

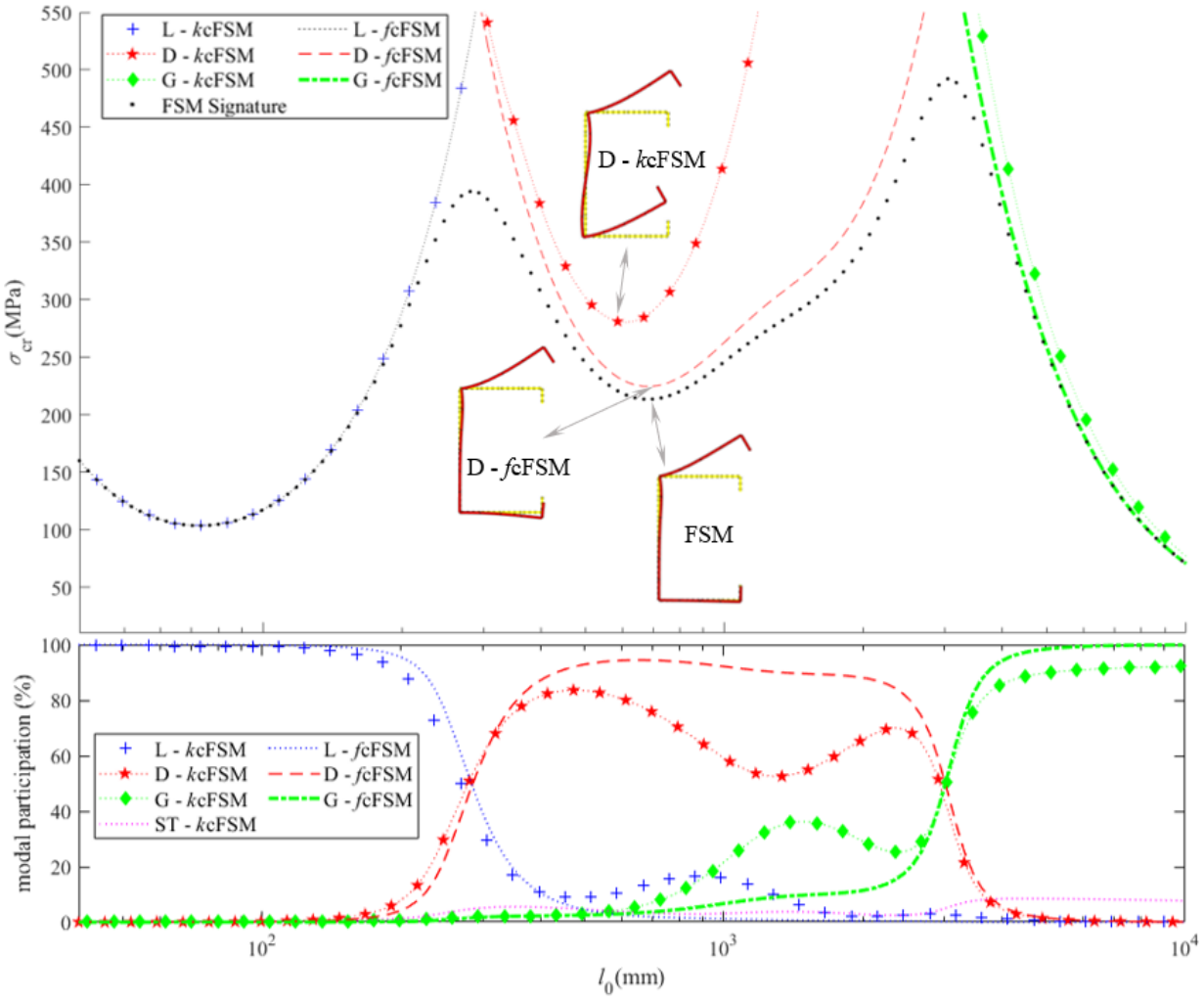

Figure 5: Signature curves and modal participations, section with elastic springs

When the buckling is dominated by L or G (i.e., small or large half-wavelengths), the constrained curves remain close to the unconstrained one, similarly to what was observed in the Section 3 example. However, in the medium length range the support springs have a significant effect. In the case of *f*cFSM the pure D and the unconstrained curves are still similar; accordingly, the *f*cFSM modal participation indicates that the buckling is dominated by distortional deformations in this region. In the case of *k*cFSM, however, the pure D signature curve runs significantly above the unconstrained one; accordingly, the *k*cFSM-based modal identification indicates strong coupling between the various modes.

4.3 Unconstrained and constrained signature curves with quasi-rigid springs

The signature curves and mode participations have been recalculated again, with considering quasi-rigid springs, with a stiffness of 10^{10} N/mm/mm. The results are summarized in Fig. 6.

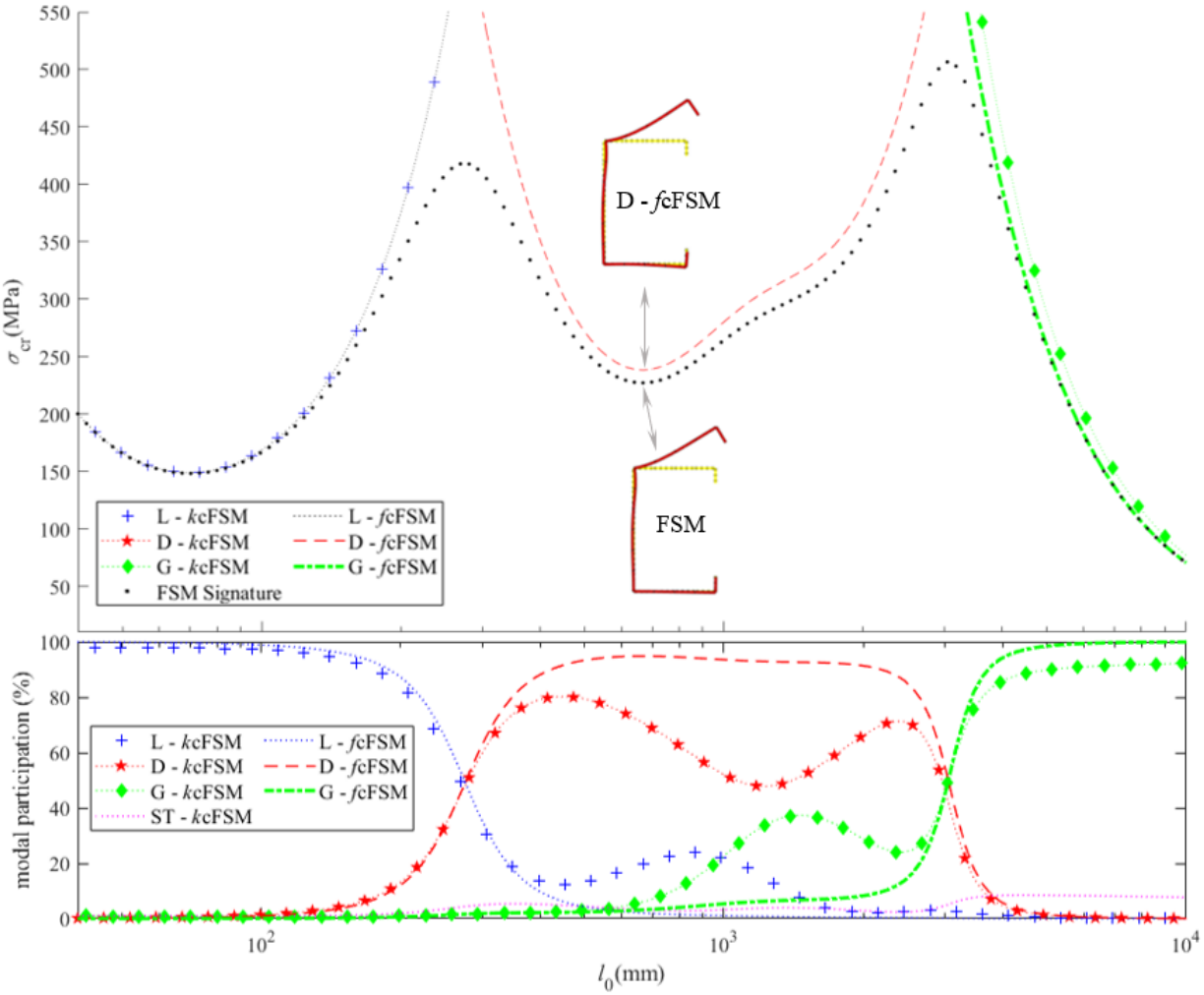

Figure 6: Signature curves and modal participations, section with quasi-rigid springs

Using quasi-rigid springs instead of the elastic ones, further modifies the results. Nevertheless, most of the previous observations remain valid, with two important differences. One, in the range of small half-wavelengths the critical values (either constrained or unconstrained) are further increased. Two, in the length of medium half-wavelengths the *k*cFSM pure D critical values become so high that the pure D curve is not visible in the plot. Remarkably, the *f*cFSM pure D curve remains close to the unconstrained curve. It is also interesting to point out that even though the *k*cFSM pure D critical values are high, the D displacement modes still exist, as clearly observable by the modal participation plots, where the D modes have important contributions.

5. Concluding remarks

In this paper two modal approaches: a kinematic-based and a force-based approach were discussed for understanding the deformations in thin-walled members. Both approaches were implemented in the context of the semi-analytical finite strip method and applied to the linear buckling analysis

of thin-walled members. The kinematic-based approach is identical to the previously developed constrained Finite Strip Method (cFSM). To distinguish between the two approaches, new acronyms were introduced: *k*cFSM for the kinematic-based cFSM and the new *f*cFSM for the force-based cFSM. The two methods were briefly presented, then discussed via numerical examples. The numerical examples show that in classic simple problems the two approaches yield nearly identical results. However, if they are applied for more complex problems, the end results differ significantly. More specifically:

- In *f*cFSM three deformation classes are distinguished, in *k*cFSM there are 4 major deformation classes, some of them divided into further sub-classes.
- While in *k*cFSM the deformation modes are dependent on the cross-section geometry only, in *f*cFSM the deformation modes may be influenced by other parameters of the member, such as supports.
- The two approaches were found to be similar in predicting global and local-plate buckling, but more significant differences were observed in the range of medium half-wavelengths, where distortional buckling governs. The results suggest that the *f*cFSM pure D modes are more similar to unconstrained FSM solutions.

Further analytical and numerical studies are in progress, as are open source tools to allow the community to utilize the different approaches.

Acknowledgments

The authors are particularly grateful to the Department of Civil and Systems Engineering (CaSE) at Johns Hopkins University. Part of this work was performed while the first author was a Visiting Faculty Scholar at CaSE, the second author a Visiting Research Scientist at CaSE, and the third a Professor at CaSE.

References

Ádány S., Schafer B.W. (2008). "A full modal decomposition of thin-walled,single-branched open cross-section members via the constrained finite stripmethod", *Journal of Constructional Steel Research*, Vol 64 (1), pp. 12-29.

Ádány S., Schafer B.W. (2014). "Generalized constrained finite strip method for thin-walled members with arbitrary cross-section: Primary modes", *Thin-Walled Structures*, Vol 84, pp. 150-169.

Ádány S., Silvestre N., Schafer B.W., Camotim D. (2009). "GBT and cFSM: two modal approaches to the buckling analysis of unbranched thin-walled members", *Int. J. Advanced Steel Construction*, Vol. 5, No. 2, pp. 195-223.

Becque J., Li, X., Davison B. (2019). "Modal decomposition of coupled instabilities: The method of the equivalent nodal forces". *Thin-Walled Structures*, Vol 143, 106229.

Beregszászi Z., Ádány S. (2019). "Modal buckling analysis of thin-walled members with rounded corners by using the constrained finite strip method with elastic corner elements", *Thin-Walled Structures*, Vol 142, pp. 414-425.

CUFSM (2023). Constrained and Unconstrained Finite Strip Method." [Online]. Available: https://www.ce.jhu.edu/cufsm/

Jin S., Li Z., Tang Q., He Z., Huang H. (2021a). "A combined force/displacement-based constrained finite strip method for modal stability analysis of thin-walled members", *Thin-Walled Structures*, Vol 159, 107322.

Jin S., Li Z., Gao T., Huang F., Gan D., Cheng R. (2021b). "Constrained shell finite element method of modal buckling analysis for thin-walled members with curved cross-sections", *Engineering Structures*, Vol 240, 112281.

Khezri M., Rasmussen K.J.R. (2019a). "An energy-based approach to buckling modal decomposition of thin-walled members with arbitrary cross sections, Part 1: Derivation", *Thin-Walled Structures*, Vol 138, pp. 496-517.

Khezri M., Rasmussen K.J.R. (2019b). "An energy-based approach to buckling modal decomposition of thin-walled members with arbitrary cross-sections, Part 2: Modified global torsion modes, examples", *Thin-Walled Structures*, Vol 138, pp. 518-531.

Nedelcu M. (2023). "New unified family of GBT deformation modes for the analysis of thin-walled cylinders", *Thin-Walled Structures*, Vol 183, 110334.